Journal of High Energy Astrophysics 26 (2020) 58–64

Contents lists available at ScienceDirect

Journal of High Energy Astrophysics

www.elsevier.com/locate/jheap

Deadtime calculation method of the High Energy X-ray telescope (HE) onboard the *Insight*-HXMT satellite

S. Xiao [a,b,*], S.L. Xiong [a,*], C.Z. Liu [a,*], X.B. Li [a], S.N. Zhang [a,b], M.Y. Ge [a], C. Cai [a,b], Q.B. Yi [a,b], Y. Zhu [a], W. Chen [a], X.F. Li [a], B. Li [a], L.M. Song [a,b], C.K. Li [a], X.Y. Song [a], Z. Chang [a], G.H. Gao [a,b], H. Gao [a,b], T.P. Li [a,b,c], Z.W. Li [a], F.J. Lu [a], X.F. Lu [a], Y.P. Xu [a,b], Y.F. Zhang [a]

[a] Key Laboratory of Particle Astrophysics, Institute of High Energy Physics, Chinese Academy of Sciences, Beijing 100049, China
[b] University of Chinese Academy of Sciences, Chinese Academy of Sciences, Beijing 100049, China
[c] Department of Astronomy, Tsinghua University, Beijing 100084, China

ARTICLE INFO

Article history:
Received 13 December 2019
Received in revised form 3 February 2020
Accepted 4 February 2020

Keywords:
Deadtime
Insight-HXMT
Gamma-ray Bursts
Terrestrial Gamma-ray Flashes

ABSTRACT

Deadtime is the time period during which a detector processes the previous photon event and any later events will be ignored, thus the calculation of deadtime is of great importance to reconstruct the incident photon flux from the recorded counts. The High Energy X-ray telescope (HE) on-board the *Insight*-HXMT satellite records the deadtime only for a fixed time bin (i.e. 1 s), therefore it is impossible to directly obtain the deadtime for an arbitrary time interval, especially for high-energy transients much shorter than one second. Based on the electronics model of HE, we establish a deadtime calculation method to derive the deadtime in any time interval. We apply this method to transient sources observed by HE, including Gamma-ray Bursts (GRB) and Terrestrial Gamma-ray Flashes (TGF). Furthermore, since the data processing capacity of HE electronics is limited, HE suffers data saturation for very bright GRBs. During the saturation period, a significant part of counts signal cannot be recorded. We find that the amount of lost counts can be estimated by comparing the recorded 1 s deadtime and the calculated deadtime using the method mentioned above.

1. Introduction

The Hard X-ray Modulation Telescope (dubbed as *Insight*-HXMT) is China's first X-ray space astronomical satellite (Li, 2007; Lu et al., 2009; Zhang et al., 2014, 2018, 2019; Cao et al., 2019; Chen et al., 2019). As one of the main payloads onboard *Insight*-HXMT, the High Energy X-ray telescope (HE) is comprised of 18 NaI (Tl)/CsI (Na) phoswich scintillator detectors, with every six detectors sharing one Analog-to-Digital Converter (ADC) (Liu et al., 2019). Photomultiplier tube (PMT) is used as the photoelectric conversion device for NaI (Tl)/CsI (Na) scintillator (the detailed structure of the detector see (Liu et al., 2019)). By adjusting the High Voltage (HV) supply of PMT, there are two modes of HE: normal mode and low gain mode. In the normal mode, the NaI (Tl) and CsI (Na) work in 20-250 keV and 80-800 keV respectively. In the low gain mode, the energy range of the CsI (Na) goes to a higher energy range of about 200-3000 keV. Note that, the CsI (Na) detectors could serve as an all-sky gamma-ray monitor in both modes (Liu et al., 2019; Li et al., 2018).

Pulse Shape Discrimination (PSD) technology is used in HE to determine whether a photon signal is produced in NaI (Tl) or CsI (Na). NaI (Tl) and CsI (Na) lead to different pulse widths because their intrinsic scintillation decay times of these two kinds of crystals are different. To define the pulse width of a signal, two points are selected on the rising and falling stages of the pulse respectively (for details see (Liu et al., 2019)), and the time interval between these two points is defined as the pulse width of the signal. Depending on the pulse width (denoted as *pw* in HE data) and pulse amplitude (denoted as *channel* in HE data), HE signals are classified into three types: (1) Normal signal: the count with pulse width less or equal to 120 and pulse amplitude greater than 20 and less than 275. Its count rate per detector ranges from a few hundreds to several thousands. Detailed information of the normal signals is recorded, including arrival time, detector ID, pulse width, pulse amplitude, etc. (2) Large signal: the count with pulse amplitude greater than 275. Its count rate is typically about a few hundred and only 1 s rates are recorded for each detector. (3) Wide signal: the count with pulse width greater than 120. Its count rate per detector varies from tens in normal mode to just a few in low gain mode. Again, only 1 s rates are recorded for each detector.

* Corresponding authors.
E-mail address: xiaoshuo@ihep.ac.cn (S. Xiao).

https://doi.org/10.1016/j.jheap.2020.02.003
2214-4048/

The accuracy of the arriving time of normal signal is determined by the sub-second module of the read-out electronics. This module uses a 500 kHz clock obtained from the frequency-divided 5 MHz clock in the satellite platform. Thus, the intrinsic time resolution of the HE normal signal is 2 μs (Liu et al., 2019).

In contrast to the fixed deadtime of 2.6 μs for normal counts and 10 μs for overflow counts utilized by *Fermi*/GBM (Meegan et al., 2009), the deadtime of HE counts signal depends on the pulse width and the pulse amplitude of the count. As shown in the ground test of HE, deadtime is less than 8 μs for normal signal and about dozens of microseconds for large or wide signal in normal mode (Liu et al., 2019).

The type of the deadtime of *Insight*-HXMT/HE is the non-paralyzable (i.e. an event happening during the deadtime is simply lost). Although there is a deadtime counter in the HE electronics to measure the total deadtime in every 1 second, deadtime for individual count signal is not registered in-flight, and the ground test only gives a rough range of deadtime for different types of signals. Therefore, it is impossible to directly calculate the total deadtime in an arbitrary time interval, such as a time period less than one second, which prevents us from doing deadtime-corrected analysis (e.g. spectroscopy) for some transient sources, such as GRBs and TGFs.

To mitigate this problem, in this paper, we develop a method to approximately calculate the deadtime of an arbitrary time period. In Section 2, we describe this method after the working principles of the HE electronics. In Section 3, we use this method to calculate the deadtime for GRBs and TGFs observed by HE. In Section 4, we extend the application of this deadtime calculation method based on deadtime information to estimate the amount of data loss when the count rate is too high to make the data transfer saturated. Finally, we give summary and discussion in Section 5.

2. The method

2.1. The HE electronics

HE consists of 18 NaI (Tl)/CsI (Na) detectors (dubbed as det#i, where i=0, 1, 2...17), and every 6 detectors share one ADC readout electronics, thus a signal in any detector will cause deadtime not only to the incident detector itself, but also to the other 5 detectors of the same ADC. The amount of deadtime depends on the type (see Fig. 1) of signal (i.e. normal, wide and large). Let's assume det#i receives a signal. When the signal pulse exceeds the preset trigger threshold, all 6 detectors of the corresponding ADC of det#i will start recording deadtime simultaneously. Before the pulse falls back to the preset threshold, if this signal is judged to be a large or wide one, then all 6 detectors except det#i will stop recording deadtime from the time of the judgment; otherwise, this signal is classified as normal and all six detectors will share the same deadtime, which is equal to the width of the pulse. To implement the Analog-to-Digital conversion, det#i will have additional deadtime, which is related to the pulse width and the pulse amplitude. In summary, a signal will cause deadtime to all 6 detectors in the same ADC, and the deadtime of the detector hit by the signal (i.e. det#i) is longer than that of the other 5 detectors.

2.2. Deadtime equation

As described above, the total deadtime in a time interval (e.g. every 1 second) recorded by a detector includes not only the deadtime of various types of signals (i.e. large, wide and normal ones) incident in this detector itself, but also the deadtime caused by signals incident in the other five detectors in the same ADC. Thus, a deadtime calculation equation for a detector (i.e. det#i) in an arbitrary time interval (δt) can be established as follows:

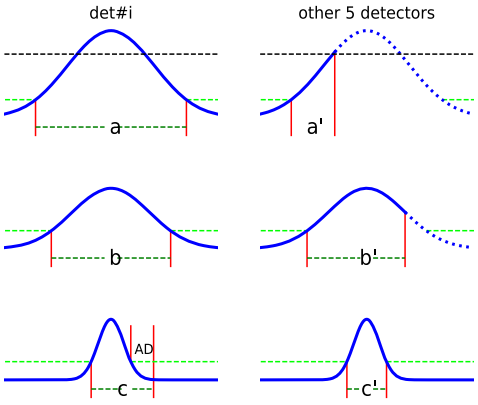

Fig. 1. Illustration of the deadtime in detectors caused by a signal incident in one detector. The solid blue lines are pulse signals, while green and black dotted lines represent preset trigger threshold and upper threshold, respectively. The dotted blue line depicts the expected pulse shape that is out of range thus not tracked by the electronics. det#i is the detector that received a signal, and other 5 detectors refer to other detectors that share the ADC with det#i. The top, middle and bottom plots are for large signal, wide signal and normal signal, respectively, while a, a', b, b', c and c' are the deadtime parameters. (For interpretation of the colors in the figure(s), the reader is referred to the web version of this article.)

$$Dt_i = a \cdot N_{l\_i} + b \cdot N_{w\_i} + c \cdot N_{n\_i} + a' \cdot N_{l\_5} + b' \cdot N_{w\_5} + c' \cdot N_{n\_5}, \quad (1)$$

where Dt_i is the total deadtime for this detector (denoted as i) in the given time interval (δt), $N_{\rm l}$, $N_{\rm w}$ and $N_{\rm n}$ are counts of large signal, wide signal and normal signal in this time interval. Subscripts of i and 5 represent the given detector and the other five detectors in the same ADC, respectively. Parameters a, a', b, b', c and c' are individual signal's deadtime for different types of signals in different detectors (see Fig. 1). Note that, individual signal's deadtime could vary from one signal to another, and here is used as the averaged deadtime over a period of time.

To use this equation to calculate the total deadtime in an arbitrary time interval, the deadtime parameters (i.e. a, a', b, b', c and c') must be derived in advance. Thanks to that the HE electronics records the total deadtime as well as the count rate of large signal and wide signal in every 1 second for every detector, we can substitute Equation (1) with the recorded total deadtime in every 1 second on the left and the recorded counts of signals in every 1 second on the right for a certain length of data (e.g. hundreds to thousands of seconds), and then these deadtime parameters (a, a', b, b', c and c') can be estimated by fitting Equation (1) using the least square method. We use $optimize.curve\_fit$ in Python to fit and derive the parameters and 1-σ errors (i.e. the confidence level is about 68%). Finally, we can use Equation (1) together with the fitted deadtime parameters to approximately calculate the total deadtime in an arbitrary time interval. Since event-by-event data are registered for normal signal, one can calculate the accurate ($N_{\rm n}$) in any time interval. However, the count rate of large ($N_{\rm l}$) and wide signal ($N_{\rm w}$) are only recorded for every 1 second, with which one must use integration and interpolation to estimate their count rates in an arbitrary time interval, especially for short time period less than 1 second.

3. Deadtime parameters

3.1. Fitting results

We fit the 1-hour data (2017-09-04T09:00-10:00 UTC) recorded by det#0, det#1 and det#16 detectors with Equation (1). HE was working in normal mode (Liu et al., 2019), and it contains 3356 seconds of data. The fit parameters are shown in Table 1. It can

Table 1
The fitting results (1-σ) of the 1-hour sample (2017-09-04 09:00-10:00 UTC).

Parameter	a (μs)	b (μs)	c (μs)	a' (μs)	b' (μs)	c' (μs)
Det#0	18.04 ± 0.40	10.08 ± 0.30	3.54 ± 0.28	2.09 ± 0.08	4.78 ± 0.10	2.24 ± 0.06
Det#1	18.90 ± 0.40	10.81 ± 0.27	2.91 ± 0.29	2.21 ± 0.08	4.46 ± 0.11	2.25 ± 0.06
Det#16	18.21 ± 0.43	12.92 ± 0.38	2.42 ± 0.30	2.57 ± 0.08	4.46 ± 0.08	2.20 ± 0.06

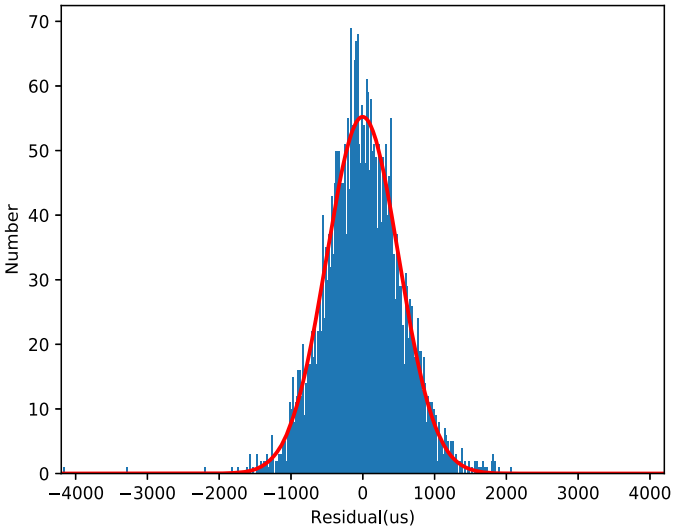

Fig. 2. Distribution of the residuals of 3356 seconds of data (2017-09-04T09:00-10:00 UTC). The red line is the fit result with a normal distribution.

be found that the parameters of different detectors are not exactly the same because of different energy spectra, but are similar.

Using the fitted parameters, the total deadtime can be calculated. Residuals of the calculated deadtime and the recorded deadtime per second are shown in the left panels of Fig. 3. It is found that almost all residuals are generally acceptable (with just a few outliers), not only for GRB 170904A (right panel in Fig. 3), but also for the whole time region (left panel in Fig. 3). Moreover, the residuals in this 1-hour data sample follows a normal distribution (see Fig. 2). The mean of the residual distribution is 7.51 μs, and the standard deviation is 516.42 μs, which is about 2% of the average total deadtime recorded per second (26268.75 μs).

3.2. Distribution of deadtime parameters

In order to study how the fitted deadtime parameters (i.e. a, a', b, b', c and c') vary with time (i.e. data sample), we collect a total of 716 data samples, including 633 samples in normal mode and 83 in low gain mode. In each sample, the length of data used to do deadtime fitting ranges from a few hundreds seconds to 3599 seconds, depending on the availability of data.

First, we calculate the relative errors of residuals (i.e. the ratio of the average of the absolute values of the residuals to the average of the recorded total deadtime per second) of these samples, and check the distribution of the residuals relative errors, as shown in Fig. 4. It is found that the relative errors are concentrated between 1.5% and 2.5%, demonstrating that this fitting approach is reasonable and the calculated deadtime using Equation (1) is a good estimation of the real deadtime (i.e. recorded deadtime).

Next, we plot the distributions of the deadtime parameters (i.e. a, a', b, b', c and c') for data samples in normal gain and low gain modes, respectively. As shown in Fig. 5, the mean deadtime to process a normal signal for the incident detector (parameter c) spans from 2.5 to 6 μs in normal mode and 3 to 4.5 μs in low gain mode.

HE detectors register the arrival time of every normal signal with a time accuracy of 2 μs. Although the deadtime of each signal varies and depends on the amplitude and width of the signal pulse (according to the HE electronics), the minimum time interval between two adjacent signals can be used as an indicator of the deadtime. As shown in Fig. 6, we calculate the minimum time interval for signals with different pulse amplitude and width, both for a single detector (det#0) and for all six detectors sharing one ADC. To ensure a sufficient statistics, ten days of data are used to make this plot. As seen from the left panel, the minimum time interval for the incident detector is 2 to 4 μs, meaning that the deadtime for incident detector to process a normal signal is between 2 μs and 6 μs. Similarly, as shown in the right panel, the minimum time interval is 0 to 2 μs, so the deadtime of the other five detectors in the ADC caused by a normal signal in the incident ranges from 0 to 4 μs. All these values are well consistent with the fitted parameters c and c' shown in Fig. 5, which gives a validation of this deadtime fitting approach.

It takes the incident detector much longer time to process large (parameter a) and wide signal (parameter b) than normal signal in both modes. However, deadtime in the other five detectors of same ADC are just several μs with the only exception of parameter b' which could go up to $\sim$ 20 μs. Moreover, deadtime for the other five detectors to process any type of signal (i.e. normal, large or wide) are always much less than that of the incident detector, which is very consistent with the working principles of the HE electronics (Fig. 1).

3.3. Deadtime proportions of signal types

Since the mean deadtime and count rates for these three types of signal (i.e. normal, large or wide) are quite different, we study how much deadtime is contributed each type of signal. We calculate each term in Equation (1) for every 1 second. Note that the deadtime varies with time (see Fig. 7), but the deadtime contributed by the large signal and the normal signal usually accounts for the majority (more than 90%).

4. Deadtime calculation for transients

The major transients that HE has detected are Gamma-ray Bursts (GRB) and Terrestrial Gamma-ray Flashes (TGF). From June 25, 2017 to November 22, 2018, *Insight*-HXMT/HE has detected 114 GRBs and dozens of TGFs Since these transients are usually very bright, especially during short peaks, deadtime estimation in arbitrary time interval, especially in sub-second timescales (e.g. from 0.1 s down to 0.1 ms), is highly demanded for light curve and spectra analysis of these transients.

Here we explain how to calculate the deadtime in any time interval. Since the deadtime parameters evolve slowly and smoothly, we fit and derive those six deadtime parameters in Equation (1) using data in a wider time region centered on the time interval of interest. For the normal signals, N_{n_i} and N_{n_5} can be calculated very accurately for arbitrary time interval because the arrival time of every normal signal is recorded. However, counts of large signals and wide signals are only recorded in every 1 second, here we assume that counts of large signals and wide signals are evenly distributed within the time interval. Then we can use the deadtime

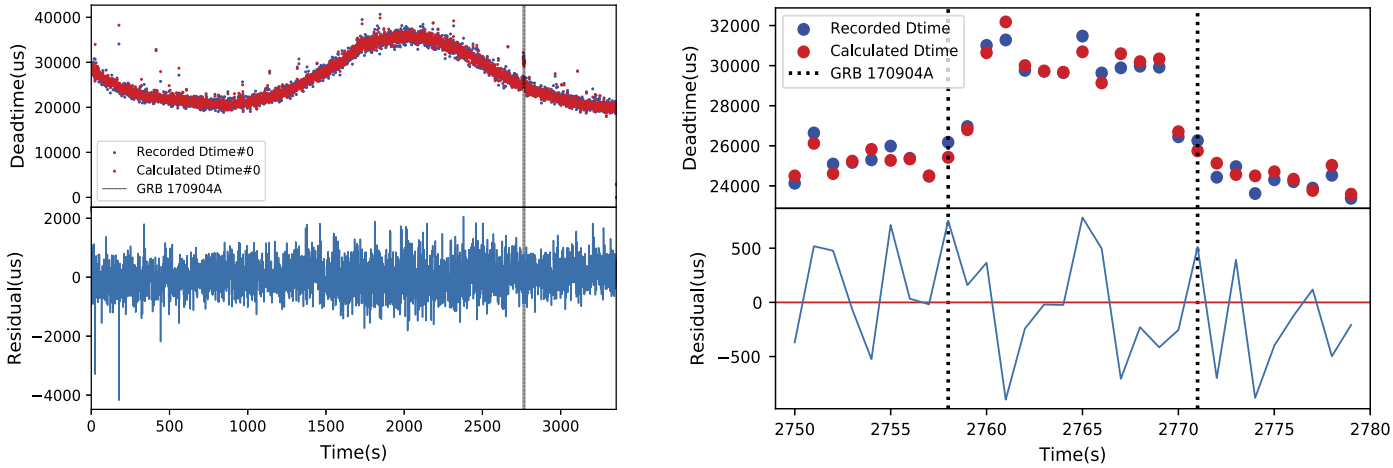

Fig. 3. (Left) In the upper panel, the red dot represents the total deadtime in each second of det#0 calculated by this method (see Equation (1)), and the blue dot represents the total deadtime in each second recorded by electronics for det#0. Lower panel shows the residuals between the recorded total deadtime and the calculated total deadtime. The vertical black dotted lines indicate the time region of GRB 170904A. Time is from 2017-09-04T09:00:00 to 2017-09-04T09:55:56 UTC. (Right) Same as the left figure but zoomed for GRB 170904A.

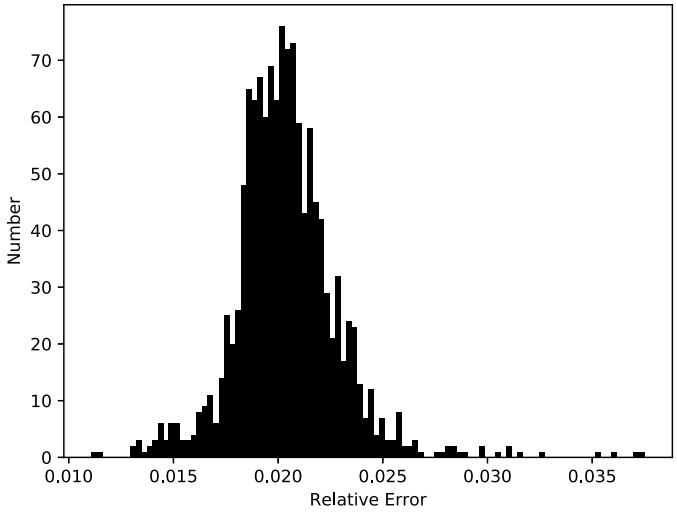

Fig. 4. Distribution of the relative errors of 716 data samples, including 633 in normal mode and 83 in low gain mode. In each sample, data in a few hundreds seconds to 3599 seconds were used. The relative error is the ratio of the average absolute values of the residuals to the average of the total deadtime per second.

Equation (1) to calculate the total deadtime for any length of time interval.

Next, we apply this deadtime calculation method to one typical TGF and one typical short GRB.

4.1. TGF 180515

TGF is a kind of gamma-ray transient with extremely high flux in very short duration (sub-millisecond) that is associated with thunderstorms and lightning (Smith et al., 2005). According to previous studies by other space detectors (e.g. CGRO/BATSE, RHESSI, *Fermi*/GBM), deadtime correction for TGF is of great importance (Grefenstette et al., 2007, 2008; Ostgaard et al.; Grefenstette et al., 2009; Gjesteland et al., 2010; Briggs et al., 2010, 2011; Stgaard et al., 2012; Briggs et al., 2013; Marisaldi et al., 2014).

Here we choose TGF 180515 as an example to do deadtime calculation. This TGF was detected by HE with a duration of about 0.2 ms. We plot its light curve together with the proportion of the deadtime in each time bin (bin width=50 μs) calculated using this deadtime calculation method (see Fig. 8). It is found that, for this TGF, the proportion of deadtime could reach as high as about 50% in some time bins, which is consistent with previous observations by other space detectors (Briggs et al., 2011; Stgaard et al., 2012).

4.2. GRB 180402A

GRB are the most luminous explosions in the universe (Mészáros, 2006), whose most energies are released in the X-ray and gamma-ray band in a duration from some milliseconds to thousands of seconds. GRBs are classified as short GRB or long GRB according to the duration of their prompt gamma-ray emission (Kouveliotou et al., 1993). In the gravitational wave multi-messenger era, short GRB is the focus of many studies since they are believed to be the probable electromagnetic counterpart of the Compact Binary Coalescence (CBC) gravitational wave events (GW).

GRB 180402A is a short GRB of T90=0.17 s observed by *Insight*-HXMT/HE, *Swift*/BAT, Konus-Wind and *Fermi*/GBM simultaneously. We plot its light curve and calculated the proportion of deadtime in each time bin (bin width=0.01 s) (Fig. 9). It can be found that, for this bright short GRB, the proportion of deadtime could go up to about 7.5%, which is not negligible in spectra analysis.

5. Lost data estimation using deadtime

Since the capacity of the data processing unit in each ADC of the HE is limited, when the count rate in one ADC is higher than its threshold, some data will be lost. Because both large signal and wide signal are just recorded as a count rate per second, their data volume is very small compared to that of normal signal, for which every count is registered, thus only normal signal will be lost.

Because this data loss happened after the deadtime accumulation electronics of HE, the total deadtime in every 1 second recorded by electronics contains contributions of not only the successfully registered but also the lost normal signals. On the other hand, the calculated deadtime only considers contributions from the successfully registered normal signals. Therefore, the difference between the calculated deadtime and the recorded deadtime can be used to estimate the lost normal signal. However, note that this loss estimation method only works for time intervals consisting of full seconds due to the recorded deadtime is for every 1 second.

Here we implement this data loss estimation method for GRB 180218A, a very bright GRB observed simultaneously by *Insight*-HXMT/HE, IPN, CALET, Konus-Wind, AstroSat CZTI and *Fermi*/GBM. We fit the data recorded by det#2, and the fitting parameters are given in Table 2. These six deadtime parameters are consistent

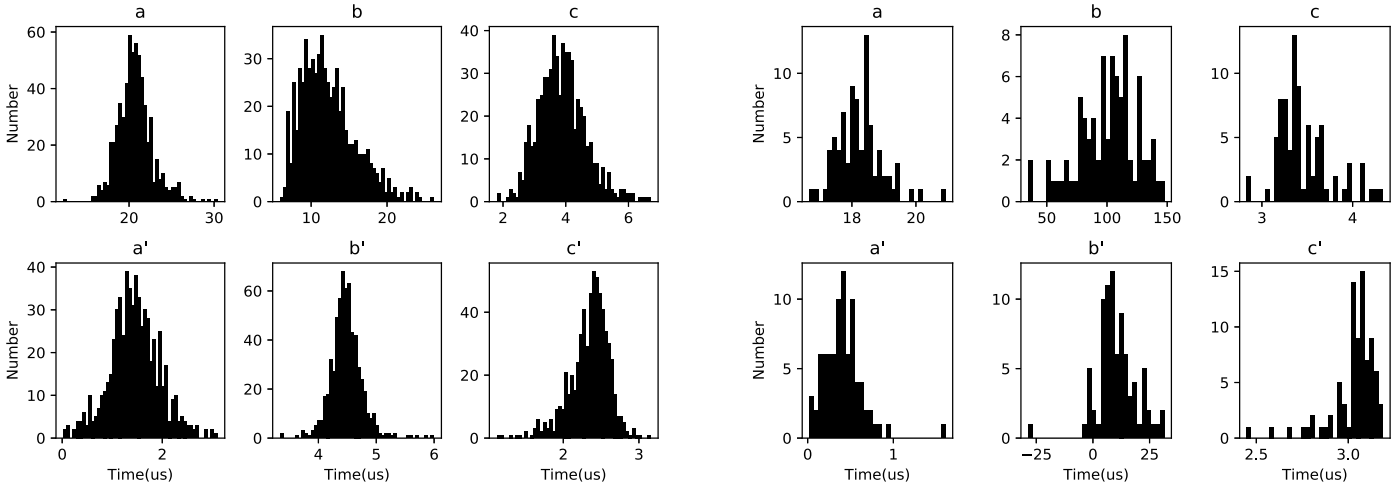

Fig. 5. Distribution of the six deadtime parameters in the equation (1) obtained by fitting 633 samples in normal mode (left) and 83 samples in low gain mode (right).

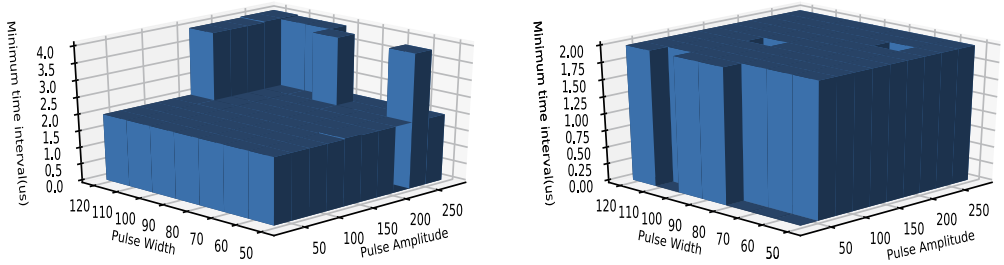

Fig. 6. The left panel is the minimum time interval of two adjacent normal signals (grouped in different pulse amplitude and pulse width) in the incident detector (det#0). The right panel is the same as left panel but for signals in the other 5 detectors in the same ADC. The bin widths of the pulse width and amplitude is 10 and 25 (see Liu et al. (2019) for details), respectively.

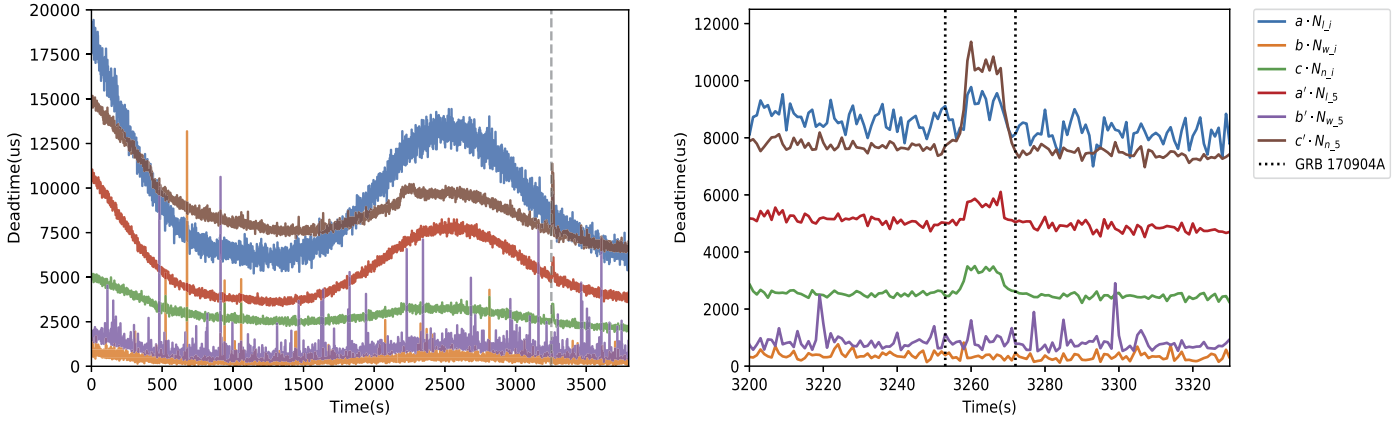

Fig. 7. Deadtime of different type of signals based on the fit results. In the left panel, the blue, the yellow, the green, the red, the purple and the brown lines represent the dead times of $a \cdot N_{l\_i}$, $b \cdot N_{w\_i}$, $c \cdot N_{n\_i}$, $a' \cdot N_{l\_5}$, $b' \cdot N_{w\_5}$ and $c' \cdot N_{n\_5}$ (in the equation (1)) of det#0 in one second, respectively. The right panel it the same as the left figure but zoomed for GRB 170904A. Time is from 2017-09-04T08:51:40 to 2017-09-04T09:55:00 UTC.

Table 2
Deadtime fitting (1-σ) results for GRB 180218A.

Parameter	a	b	c	a'	b'	c'
Value (μs)	22.67	7.78	6.54	0.95	4.35	2.02
Error (μs)	0.35	0.21	0.29	0.07	0.12	0.06

with their general distribution as shown in Fig. 5, showing that this is a reasonably good fit.

In Fig. 10, we show the recorded 1 s deadtime, the calculated deadtime for the corresponding 1 s time bin and their difference (i.e. residual). It can be found that the recorded deadtime is much longer than the calculated value during the bright part of this burst, and the maximum residual is about 8000 μs. For the 1 s time bin with the maximum residual, we further check the high time resolution (bin width of 1 ms) light curve of all six detectors sharing the same ADC with det#2, as shown in Fig. 11. It can be seen that the counts jumped abruptly to 0 in some time intervals, indicating that lots of normal signals are indeed lost.

As mentioned above, all lost counts are normal signals, and accounts for the difference between calculated dead-time and recorded dead-time in 1 s time bin. According to the electronics design, the ratio between loss counts and recorded counts should be the same for all six detectors sharing one ADC. For the 1 s time

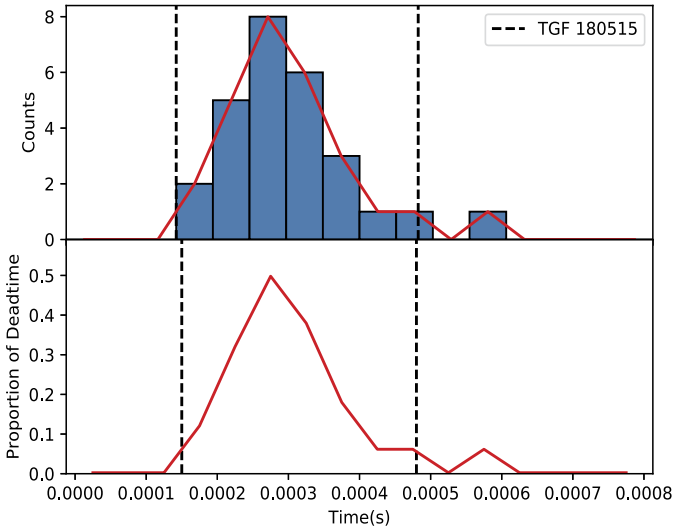

Fig. 8. Deadtime calculation for TGF 180515. The upper figure is the total light curve for detectors from #0 to #5, and the lower figure shows the proportion of deadtime in each time bin. Bin width is 50 μs. The PI range of light curve is from 0 to 255.

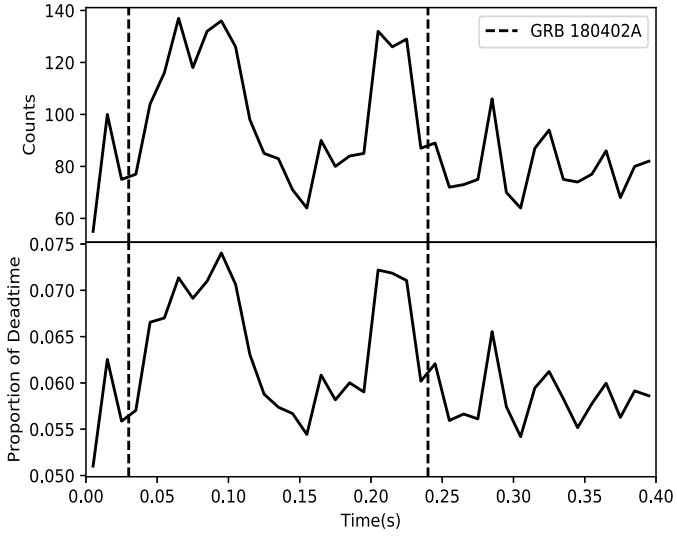

Fig. 9. Deadtime calculation for GRB 180402A. The upper figure is the total light curve for detectors from #0 to #5, and the lower figure shows the proportion of deadtime in each time bin. Bin width is 0.01 s. The PI range of light curve is from 0 to 255.

bin with the maximum residual, normal signal counts recorded by det#2 is $N_2 = 2673$, while those recorded by the other five detectors sharing the ADC is $N_5 = 10472$. We define $N_{\rm lost}$ is the number of normal signals lost by det#2 in this 1 s time bin, then $N_{\rm lost}$ can be calculated by the following equation:

$$N_{\rm lost} \cdot c + N_{\rm lost} \cdot \frac{N_5}{N_2} \cdot c' = Dt_{\rm residual}, \tag{2}$$

where c, c' are the deadtime parameters obtained by fitting (shown in Table 2) and $Dt_{\rm residual} = 7970.89$ μs is the residual deadtime. $N_{\rm lost} \cdot c$ represents the residual deadtime contributed by the lost normal signals in det#2, while $N_{\rm lost} \cdot \frac{N_5}{N_2} \cdot c'$ is the contribution of the lost normal signals in the other 5 detectors sharing the same ADC with det#2. By solving this equation, we can get $N_{\rm lost} = 553$. Thus, the total counts before data loss in det#2 should be 2673+553 = 3226, and the proportion of the lost counts in total counts is about 17%. In Fig. 12, we plot the *Fermi*/GBM light curve and the *Insight*-HXMT/HE light curves before and after the

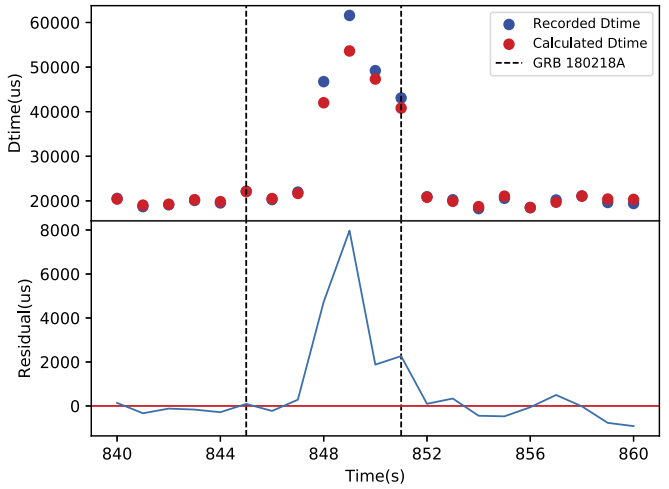

Fig. 10. Deadtime calculation for GRB 180218A. In the upper panel, the red dots represent the deadtime per second of det#2 calculated by this method, and the blue dots represent the deadtime per second recorded by det#2. The lower panel shows the residual, which is the difference between the recorded value and the calculated value. The time region between black dotted lines is the very bright GRB 180218A.

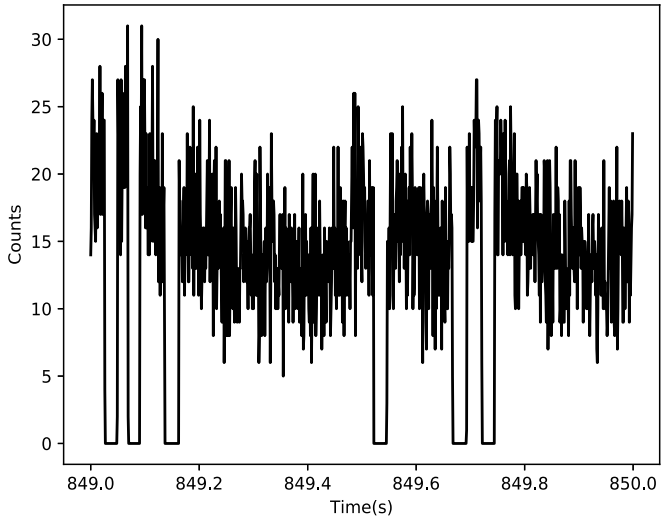

Fig. 11. High time resolution light curve of the very bright part of GRB 180218A. Time bin is 1 ms. The light curve of all six detectors (from det#0 to det#5) sharing the same ADC during the 1 s time bin with maximum residual in Fig. 10. Those time intervals where counts abruptly drop to 0 indicate the data loss due to electronics saturation of HE. The PI range of light curve is from 0 to 255.

deadtime correction; the deadtime-corrected light curve of *Insight*-HXMT/HE is obviously more similar to the *Fermi*/GBM light curve than the *Insight*-HXMT/HE light curve before the deadtime correction.

6. Summary and discussion

According to the working principle of the readout electronics of the *Insight*-HXMT/HE, we proposed a deadtime calculation method and established a deadtime equation with six parameters, which can be obtained by fitting the counts and recorded 1 s deadtime data in a certain time interval using the least squares method.

Using this deadtime calculation method, we find that the fitted deadtime parameters are consistent with both the ground test results and the minimum time interval analysis of the data, and we can calculate the deadtime in an arbitrary time interval, with a typical relative error of about 2% in 1 s timescale. Note that this

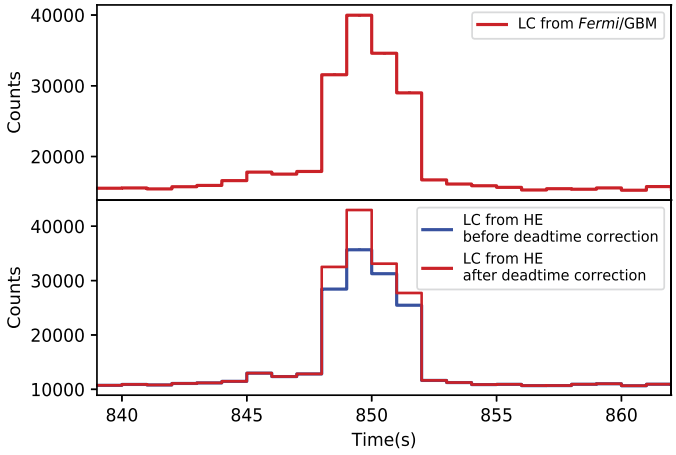

Fig. 12. Light curves of GRB 180218A. The upper panel is the summed GBM light curve for detectors n0, n1, n2, n4, n5, n7, n8, n9, na, nb, b0 and b1. In the lower panel, the blue and red lines represent the summed HE light curves for 18 detectors before and after deadtime correction, respectively. The full deposited energy range of different detectors is selected. The bin width is 1 s.

error could somewhat increase due to the uncertainty of the large and wide signal counts in sub-second timescales.

Even for those short bright GRBs detected by HE, the deadtime ratio is usually less than 10%, which indicates that the HE performance of GRB detection is very good in terms of deadtime effects. However, the deadtime ratio is usually more than 50% for TGFs, thus deadtime effects need to be carefully considered in the TGF data analysis. In addition, the deadtime effect is not only important for the spectral analysis but also for the timing analysis because it will significantly distort the power spectrum at high frequencies (Zhang et al., 1995).

We find there are some restrictions on the data which could be used for fitting. For example, when the data within about 5 minutes around the time when HE was turned on or off (such as entering and leaving the SAA area), the residual would be quite large. We consider this could be caused by the unstable electronics during these periods. For the same reason, the data within one or two minutes around the switches between the two working modes (i.e. normal mode and low gain mode) of HE can not be used either.

In the deadtime residual plot (see Fig. 3), there are couple of data points with large negative residuals, i.e. the recorded deadtime are much smaller than the calculated one. We find that this behavior occurs only in the normal mode, and such data points appear several times per hour. It is very likely that some special signals with very small amplitudes, which might not be generated by NaI (Tl)/CsI (Na), suddenly appear at these data points, and the deadtime to process this kind of special signals is much shorter than that of other normal signals. However, these six deadtime parameters are averaged values of many signals which are dominated by normal signals, thus, in the deadtime calculation, the deadtime of these special signals may be overestimated and the calculated total deadtime will be much larger than the recorded one.

Some features in the deadtime parameter distributions in both working modes of HE (see Fig. 5) are evident. Deadtime for large or wide signal is usually much larger than that of normal signal. Since the counts of wide signal N_{w_i} and N_{w_5} in Equation (1) in each second is relatively small compared to the large and normal signal, parameter b suffers larger error and spans in a much wider range. Especially the parameter b' even occasionally goes to negative value in the low gain mode, which is not physical but a mathematical solution.

Last but not least, we find that when the total count rate of HE is higher than about 30000 counts/s, counts loss usually happens due to the limited capacity of the data processing unit of the *Insight*-HXMT/HE. We proposed to estimate the amount of data loss using Equation (2). However, since only the deadtime for each 1 s time bin is recorded, data loss estimation can be done only in time intervals consisting of these 1 s time bins.

Acknowledgments

This work made use of the data from the *Insight*-HXMT mission, a project funded by China National Space Administration (CNSA) and the Chinese Academy of Sciences (CAS). The authors thank supports from the National Program on Key Research and Development Project (Grant No. 2016YFA0400801), the National Natural Science Foundation of China (Grant No. U1838201 and U1838202), and the Strategic Priority Research Program on Space Science of the Chinese Academy of Sciences (Grant No. XDB23040400). S. L. Xiong acknowledges the support from the Hundred Talent Program of Chinese Academy of Sciences.

References

Li, T.P., 2007. Nucl. Phys. B, Proc. Suppl. 166, 131.
Lu, F.J., Zhang, S., Wu, B.B., Chen, Y., Cao, X.L., Zhang, Z., Deng, J.K., Zhang, S.N., Li, T.P., 2009. AAPPS Bull. 368.
Zhang, S., Lu, F.J., Zhang, S.N., Li, T.P., 2014. Proc. SPIE 9144, 914421.
Zhang, S., Zhang, S.N., Lu, F.J., Li, T.P., Song, L.M., Xu, Y.P., Wang, H.Y., Qu, J.L., Liu, C.Z., Chen, Y., et al., 2018. Proc. SPIE 10699, 106991U.
Zhang, S.N., Li, T.P., Lu, F.J., Song, L.M., Xu, Y.P., Liu, C.Z., Chen, Y., Cao, X.L., Bu, Q.C., Cai, C., et al., 2019. Sci. China, Phys. Mech. Astron. https://doi.org/10.1007/s11433-019-1432-6. arXiv e-prints, arXiv:1910.09613.
Cao, X.L., Jiang, W.C., Meng, B., Zhang, W.c., Luo, T., Yang, S., Zhang, C.l., Gu, Y.d., Sun, L., Liu, X.j., et al., 2019. Sci. China, Phys. Mech. Astron. arXiv e-prints, arXiv:1910.04451.
Chen, Y., Cui, W.W., Li, W., Wang, J., Xu, Y.P., Lu, F.J., Wang, Y., Chen, T., Han, D.W., Hu, W., et al., 2019. Sci. China, Phys. Mech. Astron. arXiv e-prints, arXiv:1910.08319.
Liu, C.Z., Zhang, Y.F., Li, X.F., Lu, X.F., Chang, Z., Li, Z., Zhang, A., Jin, Y., Yu, H., Zhang, Z., et al., 2019. Sci. China, Phys. Mech. Astron. arXiv e-prints, arXiv:1910.04955.
Li, T.P., Xiong, S.L., Zhang, S.N., Lu, F.J., Song, L.M., Cao, X.L., Chang, Z., Chen, G., Chen, L., Chen, T.X., et al., 2018. Sci. China, Phys. Mech. Astron. 61, 031011.
Meegan, C., Lichti, G., Bhat, P.N., Bissaldi, E., Briggs, M.S., Connaughton, V., Diehl, R., Fishman, G., Greiner, J., Hoover, A.S., et al., 2009. Astrophys. J. 702, 791. arXiv:0908.0450.
Smith, D.M., Lopez, L.I., Lin, R.P., Barrington-Leigh, C.P., 2005. Science 307, 1085.
Grefenstette, B.W., Smith, D.M., Dwyer, J.R., Fishman, G.J., 2007. In: AGU Fall Meeting Abstracts, vol. 2007, AE44A–06.
Grefenstette, B.W., Smith, D.M., Dwyer, J.R., Fishman, G.J., 2008. Geophys. Res. Lett. 35, L06802.
Ostgaard, N., Gjesteland, T., Connell, P.H., Stadsnes, J., In: EGU General Assembly Conference Abstracts, 2009, p. 9504.
Grefenstette, B.W., Smith, D.M., Hazelton, B.J., Lopez, L.I., 2009. J. Geophys. Res.
Gjesteland, T., Østgaard, N., Connell, P.H., Stadsnes, J., Fishman, G.J., 2010. J. Geophys. Res. Space Phys. 115, A00E21.
Briggs, M.S., Fishman, G.J., Connaughton, V., Bhat, P.N., Paciesas, W.S., Preece, R.D., Wilson-Hodge, C., Chaplin, V.L., Kippen, R.M., von Kienlin, A., et al., 2010. J. Geophys. Res. Space Phys. 115, A07323.
Briggs, M.S., Connaughton, V., Wilson-Hodge, C., Preece, R.D., Fishman, G.J., Kippen, R.M., Bhat, P.N., Paciesas, W.S., Chaplin, V.L., Meegan, C.A., et al., 2011. Geophys. Res. Lett. 38, L02808.
Stgaard, N., Gjesteland, T., Hansen, R.S., Collier, A.B., Carlson, B., 2012. J. Geophys. Res. Space Phys. 117, A03327.
Briggs, M.S., Foley, S., Tierney, D., Fitzpatrick, G., Chaplin, V., McBreen, S., Connaughton, V., 2013. In: AGU Fall Meeting Abstracts, vol. 2013, AE23A–0417.
Marisaldi, M., Fuschino, F., Tavani, M., Dietrich, S., Price, C., Galli, M., Pittori, C., Verrecchia, F., Mereghetti, S., Cattaneo, P.W., et al., 2014. J. Geophys. Res. Space Phys. 119, 1337.
Mészáros, P., 2006. Rep. Prog. Phys. 69, 2259. arXiv:astro-ph/0605208.
Kouveliotou, C., Meegan, C.A., Fishman, G.J., Bhat, N.P., Briggs, M.S., Koshut, T.M., Paciesas, W.S., Pendleton, G.N., 1993. Astrophys. J. 413, L101.
Zhang, W., Jahoda, K., Swank, J., Morgan, E., Giles, A., 1995. Astrophys. J. 449, 930.